Comparison of Intratumoral Distribution of ^{99m}Tc-MIBI and Deoxyglucose in Mouse Breast Cancer Models

Hiromichi Ohira, Kazuo Kubota, Noriaki Ohuchi, Yukou Harada, Hiroshi Fukuda, and Susumu Satomi

Second Department of Surgery, Tohoku University School of Medicine, Sendai; and Department of Nuclear Medicine and Radiology, Institute of Development, Aging and Cancer, Tohoku University, Sendai, Japan

The aims of this study were to evaluate the distribution of ^{99m}Tc-methoxyisobutylisonitrile (MIBI) in 3 animal models of breast cancer, the effect of radiotherapy on ^{99m}Tc-MIBI uptake, and the relationship between uptake and microvessel density. **Methods:** We used syngeneic, subcutaneously transplanted FM3A, MM48, and Ehrlich mouse breast cancer. ^{99m}Tc-MIBI and FDG were injected intravenously, and tumor uptake was measured 30 min later. Double-tracer macroautoradiography (ARG) images were prepared with ^{99m}Tc-MIBI and 2-deoxy-D-[1-^{14}C]-glucose (^{14}C-DG), analyzed quantitatively, and compared with histology. The radiotherapeutic effects of 20 Gy x-ray irradiation were monitored by measuring tumor volume, tumor uptake, and ARG findings using ^{99m}Tc-MIBI and FDG in FM3A tumors. Microvessel density was quantified by immunohistochemical staining for CD34 and compared with ARG using ^{99m}Tc-MIBI in FM3A tumors. **Results:** FM3A, MM48, and Ehrlich tumors showed different growth rates and radiosensitivities. Uptake of FDG, but not of ^{99m}Tc-MIBI, correlated significantly with growth rates. Compared with ^{14}C-DG, ^{99m}Tc-MIBI accumulated more in cancer cells and less in infiltrating fibroblasts and macrophages in all tumor models. Irradiation significantly decreased ^{99m}Tc-MIBI uptake, but a rapid increase was noted at recurrence on day 7. Changes in FDG uptake were not significant at recurrence. Microvessel density in tumor tissue correlated significantly with ^{99m}Tc-MIBI uptake on ARG. **Conclusion:** Accumulation of ^{99m}Tc-MIBI in cancer cells is preferential and can be used as a sensitive marker to examine the response to radiotherapy. Angiogenesis seems to enhance accumulation of ^{99m}Tc-MIBI in tumors. These characteristics may be favorable for tumor imaging using ^{99m}Tc-MIBI.

Key Words: ^{99m}Tc-methoxyisobutylisonitrile; deoxyglucose; breast cancer; autoradiography; microvessel

J Nucl Med 2000; 41:1561–1568

Breast cancer is the leading cause of death among women in developed countries, and the incidence of breast cancer remains high (*1*). ^{99m}Tc-methoxyisobutylisonitrile (MIBI) is a tracer that is widely used as a myocardial perfusion agent. Since the publication of the first study on ^{99m}Tc-MIBI uptake in breast cancer in 1992 (*2*), there has been continued interest in the evaluation of breast cancer using this radiopharmaceutical agent. Various groups have reported the clinical usefulness of ^{99m}Tc-MIBI scintimammography. In particular, ^{99m}Tc-MIBI scintimammography has been used to detect tumors in patients with dense breasts, to evaluate chemotherapeutic response, and to predict multidrug resistance (*3–6*). Cellular accumulation of ^{99m}Tc-MIBI has been shown to correlate with the level of P-glycoprotein expression. P-glycoprotein, a product of the *mdr* gene, is well known to actively expel ^{99m}Tc-MIBI from tumor cells through an efflux pump using adenosine triphosphate (*5,7–9*). However, only a few studies have evaluated the accumulation and distribution of ^{99m}Tc-MIBI within tumors negative for P-glycoprotein.

Angiogenesis is an important process in the proliferation and metastasis of breast carcinoma (*10–13*), and immunohistochemically determined microvessel density has been used as a prognostic indicator of breast cancer (*11–13*). However, to our knowledge, the correlation between angiogenesis and the magnitude of tumor ^{99m}Tc-MIBI uptake has not been evaluated.

Our aim was to evaluate intratumoral accumulation and distribution of ^{99m}Tc-MIBI and to compare it with either 2-deoxy-D-[1-^{14}C]-glucose (^{14}C-DG) or FDG using 3 animal models of breast cancer. We also investigated the effects of irradiation on ^{99m}Tc-MIBI uptake and evaluated the correlation between microvessel density and ^{99m}Tc-MIBI uptake.

MATERIALS AND METHODS

Tumor Growth Study

The experimental protocol was approved by the Laboratory Animal Care Committee of Tohoku University. Female 6-wk-old C3H/He or DDY mice received in their left thighs 0.1-mL subcutaneous injections of a suspension containing between 0.5×10^7 and 1.5×10^7 cells of syngeneic mouse breast cancer models of FM3A, MM48, and Ehrlich. The solid tumors were measured daily using vernier calipers. The product of the 3 principal diameters of each tumor was designated as tumor volume. Irradiation was performed when the tumor diameter reached approximately 10 mm. The mice were anesthetized with an intraperitoneal injection of 1 mg sodium

Received Oct. 29, 1999; revision accepted Feb. 16, 2000.

For correspondence or reprints contact: Kazuo Kubota, MD, Department of Nuclear Medicine and Radiology, Institute of Development, Aging and Cancer, Tohoku University, 4-1 Seiryo-machi, Aoba-ku, Sendai, 980-8575, Japan.

pentobarbital and then were positioned with adhesive tape to place the tumor-bearing thigh in the field of irradiation. The other parts of the body were left outside the field (*14*). Tumors were exposed to a single dose of 20 Gy x-rays (150 kV, 20 mA) using experimental irradiation equipment (MBR-1520R, Hitachi Medical Co., Japan) at a rate of 1.50 Gy/min (at 65-cm source–skin distance and 1-cm depth) with a 1-mm aluminum filter to remove low-energy x-rays and to homogenize the dose distribution. Nonirradiated tumors in mice that were handled in the same manner were used as controls. Eight irradiated mice and 8 nonirradiated mice were used for the tumor growth study.

Tumor Uptake Study

The FM3A, MM48, and Ehrlich tumor uptake study was performed when the volume of each tumor was approximately 1000 mm^3 (approximately 10 mm in diameter). Seven mice bearing tumors in both thighs were used for each type of tumor, for a total of 21 mice. After the mice had fasted for 6 h, 555 kBq (15 μCi) FDG (radiochemical purity > 99%) and 740 kBq (20 μCi) ^{99m}Tc-MIBI (Daiichi Radioisotope Laboratories, Tokyo, Japan) were mixed in 0.25 mL saline and injected through the lateral tail vein. FDG was synthesized using an automated system (*15*). Thirty minutes later, the mice were killed by an overdose of anesthesia. Tumor samples were quickly dissected, excised, and weighed, and ^{18}F was measured by an automated γ scintillation counter with a window of 450–600 keV just after sampling. No ^{99m}Tc radioactivity spilled over to the window of ^{18}F. Twenty-four hours later, when ^{18}F (half-life, 109.7 min) had decayed to 0.01%, ^{99m}Tc was measured with a window of 70–180 keV. ^{99m}Tc was counted without contamination of ^{18}F radioactivity at that time. Tumor radioactivity was expressed as percentage injected dose (%ID) per gram, which equals ([tissue counts per minute/tissue weight in grams]/injected dose counts per minute) × 100.

We did not estimate the expression of tumor radioactivity per unit of body weight, because the 6-wk-old female C3H/He and DDY mice were handled in the same manner and were of similar body weight.

Double-Tracer Macroautoradiography

Approximately 10 d after tumor cell transplantation, C3H/He mice with FM3A and MM48 tumors and DDY mice with Ehrlich tumors received intravenous injections of a mixture of 111 MBq (3 mCi) ^{99m}Tc-MIBI and 370 kBq (10 μCi) ^{14}C-DG (American Radiolabeled Chemicals, Inc., St. Louis, MO). The specific activity was 2.04 GBq/mmol, and the radiochemical purity was more than 99%. In preliminary studies, we determined the linear correlation between the radioactivity and the autoradiographic density of ^{99m}Tc, a pure γ emitter, and selected 111 MBq per mouse as the injection dose for macroautoradiography (ARG). A linear relationship between the density on ARG and the actual radioactivity has been reported for ^{14}C (*16*) using the same ARG experimental system. In this study, ARG was performed within the confirmed range of linearity.

The mice were killed by an overdose of chloroform at 30 min. This time point was determined through a time-course tissue distribution experiment. The tumors were dissected and embedded in a frozen block with a medium (O.C.T. compound; Miles Inc., Elkhart, IN), and the sample blocks were sectioned on a cryostat at −25°C (*16,17*). Sections (10 μm thick) were mounted on clean glass slides, air dried, and placed in direct contact with ARG films (BioMax MR; Kodak, Rochester, NY) for 6 h to produce ^{99m}Tc-MIBI images. Three days later (approximately 12 half-lives of ^{99m}Tc), when ^{99m}Tc had decayed, the same sections were placed in contact with other films for 7 d to produce ^{14}C-DG images. Sections on the slides were stained with hematoxylin-eosin and examined under an optical microscope.

Analysis of ARG

Intratumoral distribution of 2 tracers within the same sections was analyzed using coregistered double-tracer ARG images and image analysis software (Win ROOF, version 3.21; Mitani Corp., Fukui, Japan). ARG images were computerized using a charged coupled device camera system (FUJI HC-300/OL; Fuji Photo Film Co., Tokyo, Japan), then stored as 1280 × 1000 pixel 8-bit images (256 gray scale). Intratumoral tissue components were covered with a square region of interest (ROI) ranging from 0.5 × 0.5 to 2.0 × 2.0 mm for comparative histology. Quantitative evaluation of ARG was performed by measuring the optical density in the ROIs after background subtraction. This measurement was followed by analysis of the regional radioactivity of the 2 tracers in the same ROI in the same section.

FDG Uptake Study and ^{99m}Tc-MIBI After Irradiation

We used the FM3A tumor for this study. Four groups, each containing 6 mice, were administered FDG and ^{99m}Tc-MIBI 2, 4, or 7 d after irradiation. Mice of another group (n = 6) were not irradiated and served as controls (day 0). X-ray irradiation was performed using the same method as for the tumor growth study. Thirty minutes after injection of FDG and ^{99m}Tc-MIBI, tumors were excised from each of 24 mice, and blood samples were withdrawn by heart puncture.

ARG After Irradiation

Two days after exposure to 20 Gy of single-dose x-ray irradiation, FM3A tumors were prepared for ARG using the same method as described above. Double-tracer ARG images with ^{99m}Tc-MIBI and ^{14}C-DG were prepared similarly, and the sections were processed for hematoxylin-eosin staining and microscopic evaluation.

Microvessel Immunohistochemical Staining and ^{99m}Tc-MIBI ARG

Microvessels in tumor tissues were identified by staining endothelial cells with mouse monoclonal antibody against CD34 (Nichirei Co., Tokyo, Japan) (*13,18,19*). Briefly, 10-μm-thick sections of frozen FM3A tumors were mounted on poly-L-lysine–coated microscope slides, air dried, fixed in acetone at 4°C for 10 min, and processed for ARG of ^{99m}Tc-MIBI as described above. The same sections were processed for standard avidin-biotinylated peroxidase complex methods after the incubation with monoclonal antibody to microvessel CD34. Diaminobenzidine was used as a chromogen (Vector Laboratories, Burlingame, CA). For negative controls, sections were prepared without using the primary antibody.

Sections of FM3A tumors were examined for the density of microvessels and the radioactivity of ^{99m}Tc-MIBI. Initially, 3 areas of each section were classified according to the microvessel density in the tumor at low magnification (×20 and ×100) as high, intermediate, or low. Then, individual microvessels in the classified areas were counted on a ×400 field (0.09 mm^2 per field). Any brown-stained endothelial cell or cell cluster that was clearly separate from adjacent microvessels, cancer cells, and other connective tissue elements was considered a single, countable

microvessel. Each count was expressed as the number of microvessels identified within a ×400 field and expressed per square millimeter.

^{99m}Tc-MIBI ARG images were analyzed on a computer. Individual areas of images corresponding to microvessel density grade in the same section were covered with square ROIs (each ROI was 0.4 × 0.4 mm), and quantitative evaluation was performed as described above. Then, the regional radioactivity of ^{99m}Tc-MIBI ARG of the corresponding microvessel density grade at the same section was plotted. The correlation coefficient of the relationship between optical density on ^{99m}Tc-MIBI and microvessel density was computed.

TABLE 1
Comparison of Uptake by Tumors

Tumor	FDG	^{99m}Tc-MIBI
FM3A	8.50 ± 1.03*	1.41 ± 0.33
MM48	9.63 ± 1.91*	1.18 ± 0.69
Ehrlich	4.73 ± 1.18*	1.75 ± 0.26

*$P < 0.001$, Fisher test.
Data are expressed as mean %ID/g ± SD of 14 mice 30 min after injection.

RESULTS

Effect of Irradiation on Tumor Growth Curve

Figure 1 shows the effect of irradiation on the growth curve of each tumor. MM48 tumors were the most radioresistant; these continued to increase in volume even after 20 Gy irradiation.

FDG and ^{99m}Tc-MIBI Tumor Uptake Study

Table 1 shows the uptake of FDG and ^{99m}Tc-MIBI 30 min after injection. Tumor uptake of FDG was higher than that of ^{99m}Tc-MIBI for all types of tumors. A comparison of the uptake of the 2 tracers showed that uptake was highest for MM48 tumors (the most rapidly growing and radioresistant type), lower for FM3A tumors, and lowest for Ehrlich tumors (a slow-growing and radiosensitive type). Differences in the uptake pattern of FDG among the 3 tumors were statistically significant ($P < 0.001$). In contrast, ^{99m}Tc-MIBI showed a similar accumulation in each type of tumor.

Double-Tracer ARG with ^{99m}Tc-MIBI and ^{14}C-DG

Figure 2 shows representative ARG images of ^{99m}Tc-MIBI and ^{14}C-DG in the double-tracer study, the corresponding histologic tumor sections, and sketches of the photomicrographs.

Optical Density of Different Tissue Components

Figure 3 shows the results of ARG with ^{99m}Tc-MIBI and ^{14}C-DG images. Table 2 compares the uptake of 2 tracers by viable cancer cells and connective tissue. The ratio of viable cancer cells to connective tissue on ^{99m}Tc-MIBI images was significantly higher than on ^{14}C-DG images for all tumors ($P < 0.05$ for FM3A and Ehrlich; $P < 0.001$ for MM48). These results suggest that intratumoral accumulation of ^{99m}Tc-MIBI represents the presence of viable cancer cells more preferentially than does intratumoral accumulation of ^{14}C-DG.

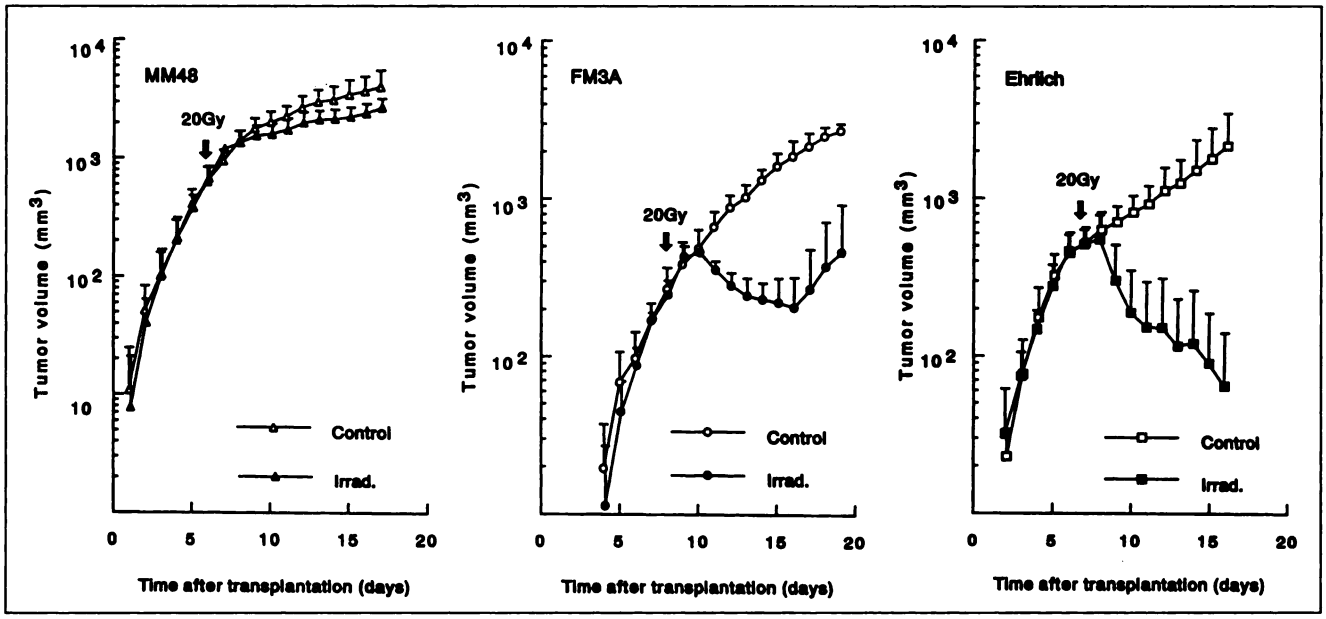

FIGURE 1. Tumor growth curve after single dose of 20 Gy irradiation (Irrad.). Day 0 is when tumor cells were inoculated in thighs of mice. Irradiation was performed on day 6 for MM48 tumors, day 8 for FM3A tumors, and day 7 for Ehrlich tumors. Changes in tumor volume are plotted on logarithmic scale against time on linear scale. Each point represents mean of 8 tumors. Pattern of FM3A tumor growth shows swelling for 2 d after irradiation (days 9 and 10), followed by shrinkage until day 16 (8 d after irradiation) and regrowth on day 17 (9 d after irradiation). Ehrlich tumors show radiosensitivity, which regresses soon after irradiation and becomes unmeasurable on day 17 (10 d after irradiation). MM48 shows rapid growth, with tumor volume doubling in approximately 2.0 d. For FM3A and Ehrlich, volume doubling time was approximately 2.5 and 3.8 d, respectively, as measured from time of irradiation.

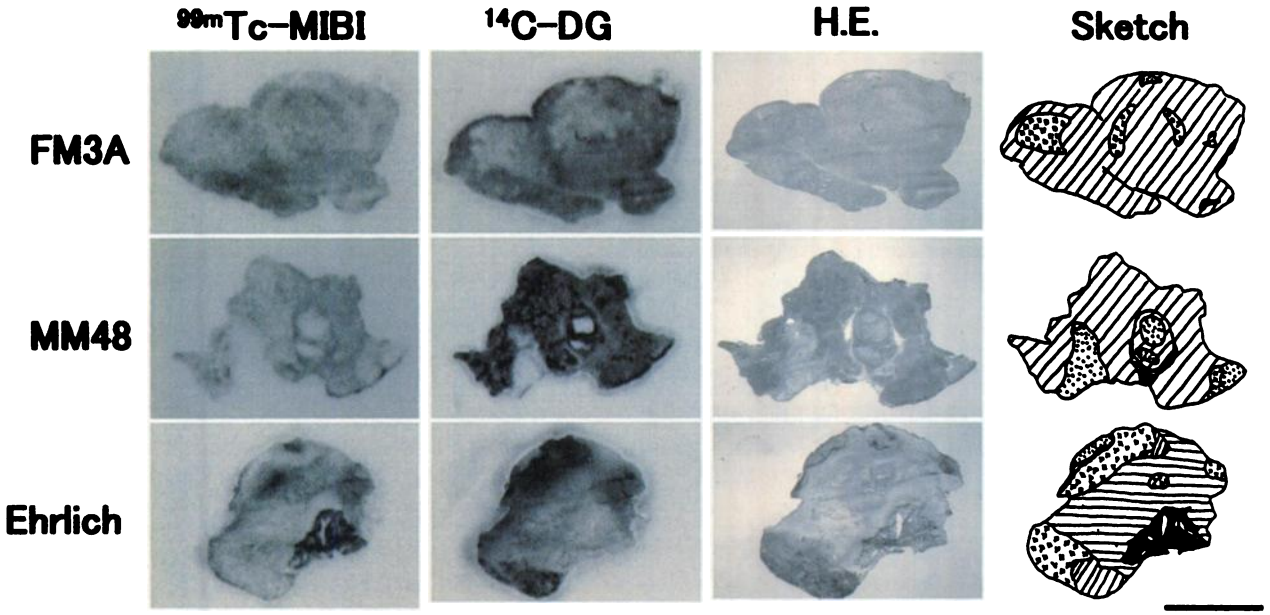

FIGURE 2. ARG images of ^{99m}Tc-MIBI and ^{14}C-DG distribution, photomicrograph of specimen stained with hematoxylin-eosin (H.E.) used for production of ARG image, and sketch of photomicrograph. In top row, FM3A tumor shows similar uptake pattern for ^{99m}Tc-MIBI and ^{14}C-DG. Histologic examination showed viable cancer cells occupying almost the whole tumor and dense area on both ARG images corresponding to viable cancer cells. In middle row, MM48 shows higher uptake of both tracers by viable cancer cells than by degenerating cancer cells and connective tissue. Almost no tracer accumulation is seen in necrotic tissue in both images. In bottom row, muscle has highest ^{99m}Tc-MIBI uptake, and accumulation in viable and degenerating cancer cells is slight. ^{14}C-DG is accumulated largely within cancer cells, whereas muscle and connective tissue show equal tracer accumulation. Each tracer showed little uptake by necrotic tissue. ▨ = viable cancer cells; ▤ = degenerating cancer cells; ▤ = connective tissue; ▩ = necrotic tissue; ■ = muscle. Scale bar is 5 mm.

Uptake Study of FDG and ^{99m}Tc-MIBI After Irradiation

At our laboratory, previous time-course studies of the distribution of FDG uptake in tissues showed that a transient rise in blood levels 1 min after injection was followed by a rapid decrease and, afterward, a persistently low uptake (*20*). In a series of preliminary experiments, we confirmed that ^{99m}Tc-MIBI levels in blood decreased within 5 min after injection and remained low and stable. Therefore, we considered the %ID of blood as the background value. To compensate for large differences in the absolute value of FDG and ^{99m}Tc-MIBI, and to compare the changes in the uptake pattern after radiotherapy, tumor uptake data were expressed as the tumor-to-blood ratio (%ID of tumor/%ID of blood).

In Figure 4, FM3A tumor-to-blood ratios of the 2 tracers are compared after a single irradiation dose of 20 Gy. The results suggest that regrowth of FM3A after radiotherapy is detected as an earlier increase in ^{99m}Tc-MIBI uptake than in FDG uptake, in addition to changes in tumor volume.

ARG of Irradiated Tumors

Figure 5 shows double-tracer ARG of an FM3A tumor and a histologic section. Differences in uptake pattern were seen between ^{99m}Tc-MIBI and ^{14}C-DG in the same section. An accumulation of ^{14}C-DG in areas containing fibroblasts and macrophages, in addition to areas containing viable cancer cells, influenced radiotherapy and explains the ^{14}C-DG uptake pattern in ARG. The dense ring on the ^{99m}Tc-MIBI image consisted of almost all viable cancer cells, and the low-uptake areas inside the hot areas consisted of both viable cancer cells and damaged cells with swollen nuclei and cytoplasm, pyknotic changes such as apoptosis, and abnormal mitosis because of radiotherapy (*21*). These findings suggest that ^{99m}Tc-MIBI accumulates in areas of little irradiation damage but not in areas of severe damage.

Correlation Between Microvessel Density and Optical Density of ^{99m}Tc-MIBI ARG

A total of 32 slides were stained, and microvessel counts were satisfactory in 24. The other 8 could not be evaluated because of low stain intensity, high background staining, or insufficient FM3A tumor tissue for microvessel counting. As Figure 6 shows, areas of high neovascularization were not distributed in a specific area of the tumor, although they were most frequently noted at the tumor periphery. Areas containing myocytes were excluded, because the optical density was high (Fig. 2). The mean (±SD) microvessel count was 21.9 ± 11.7 per ×400 field (median, 20; range, 4–69; n = 72) and the mean optical density was 21.9 ± 15.6 per pixel (median, 18.4; range, 2.1–51.8; n = 72). Figure 7 shows a linear and significant correlation between microvessel density in FM3A tumors and the optical density of ^{99m}Tc-MIBI ARG in the same sections ($r = 0.592$; $P < 0.0001$; n = 72).

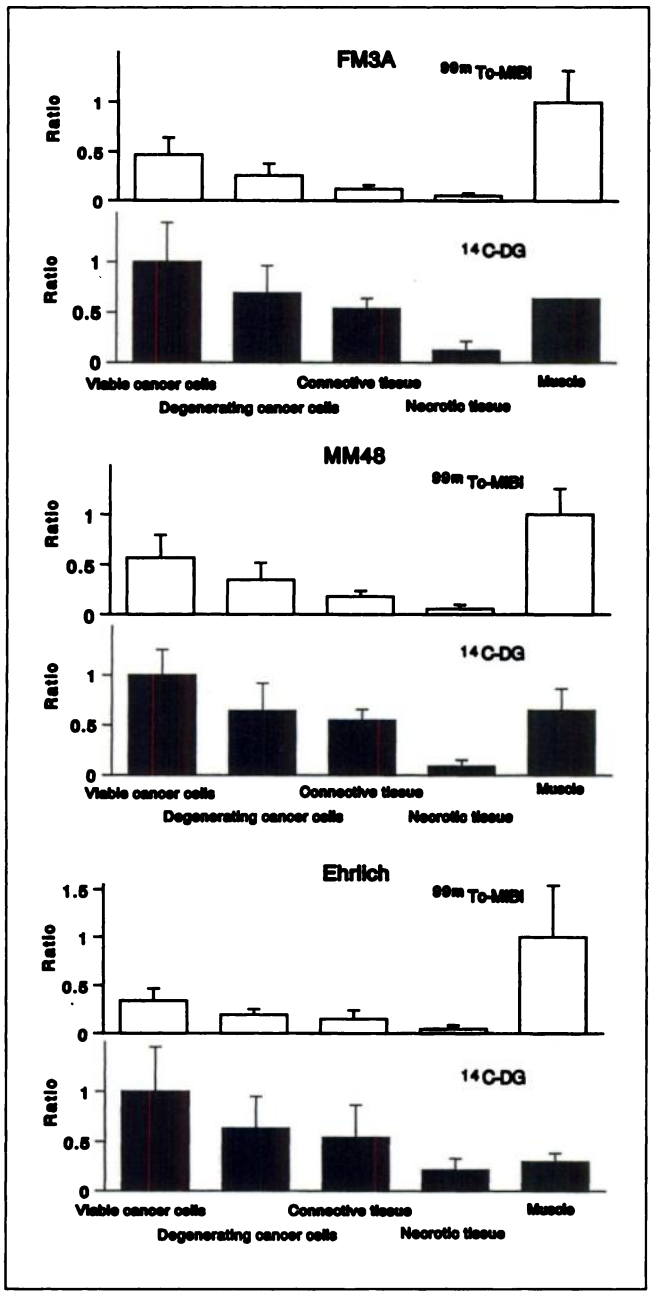

FIGURE 3. Comparison of intratumoral cellular uptake ratio among 3 tumors. Uptake is expressed relative to highest uptake of ^{99m}Tc-MIBI and ^{14}C-DG in tissue component 30 min after injection. ^{99m}Tc-MIBI shows higher uptake by muscle than by other components for all tumor models, whereas ^{14}C-DG shows very high uptake by viable cancer cells. Necrotic tissue has lowest uptake of both tracers for all tumors. ^{99m}Tc-MIBI shows similar intratumoral distribution pattern irrespective of tumor characteristics.

DISCUSSION

A study has shown that the accumulation of ^{99m}Tc-MIBI within mitochondria is caused by the electric potentials generated across mitochondrial membranes (*22*). Because malignant tumors maintain a more negative transmembrane potential, ^{99m}Tc-MIBI accumulation increases in these tissues (*23,24*). Furthermore, other studies have shown that the organotechnetium complex, ^{99m}Tc-MIBI, a lipophilic cationic radiopharmaceutical, is a suitable transport substrate for P-glycoprotein (*5,7*). However, the distribution characteristics of ^{99m}Tc-MIBI and its ARG findings have not been reported previously, because ^{99m}Tc provides a pure γ emission that radiates through a contact ARG film. Recently, FDG PET has been used not only for the detection of malignant tumors but also for the assessment of chemothera-

TABLE 2
Comparison of Optical Density on Background-Corrected ARG Images

Tumor	^{99m}Tc-MIBI	^{14}C-DG
FM3A	3.18 ± 1.22*	1.79 ± 0.52
MM48	3.62 ± 0.97†	1.74 ± 0.11
Ehrlich	2.87 ± 1.00*	1.75 ± 0.26

*$P < 0.05$.
†$P < 0.001$.
Values are mean ratio of viable cancer cells to connective tissue ± SD in 6–12 mice. Student *t* test was used for FM3A data, and Welch's *t* test was used for MM48 and Ehrlich data.

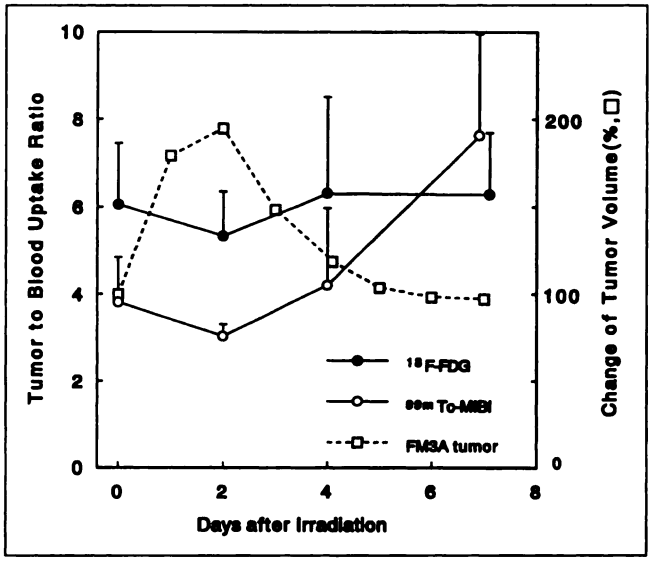

FIGURE 4. Dynamic changes in FM3A tumor uptake for FDG and ^{99m}Tc-MIBI and tumor volume for 7 d after single dose of 20 Gy x-ray irradiation. Nonirradiated group is represented by data at day 0. Data are mean and SD of 6 mice. Tumor volume is plotted as mean value for reference (mean and SD are shown in Fig. 1). In nonirradiated control tumors, FDG uptake (solid line) is higher than ^{99m}Tc-MIBI uptake (broken line). FDG and ^{99m}Tc-MIBI uptake show similar dynamic changes until day 4, consisting of gradual decrease on day 2 to 88.0% ± 16.8% and 79.9% ± 7.1%, respectively, of control level. Thereafter, uptake of both tracers increases gradually on day 4 to 104% ± 36.4% and 110% ± 46.1%, respectively, of control level. FDG uptake does not change (104% ± 23.2% of control level) on day 7, whereas ^{99m}Tc-MIBI uptake increases progressively on day 7 to twice control level (199 ± 61.0% of control level) and is also higher than FDG uptake.

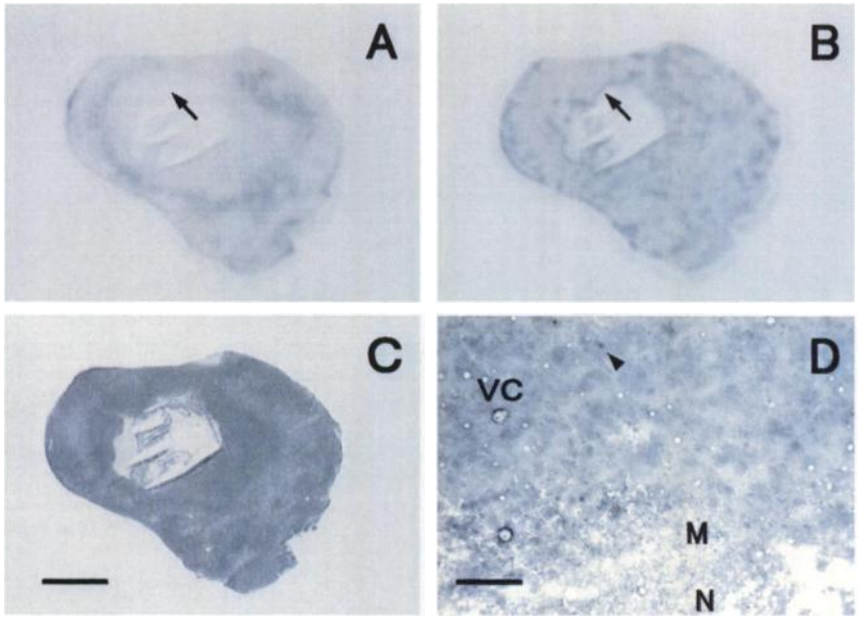

FIGURE 5. ARG images with ^{99m}Tc-MIBI (A) and ^{14}C-DG (B), and corresponding histology of FM3A tumor (C), 2 d after irradiation. ^{14}C-DG ARG shows central, low-density area of necrosis and ^{14}C-DG uptake in viable tissue, with scattered spots and intense ring in periphery. ^{99m}Tc-MIBI ARG does not show high density in ring of viable tissue but shows another ring of high density outside, in middle of viable tissue. Magnification (×200) of area indicated by arrow shows pyknotic changes (arrowhead) (D) and presence of viable cancer cells (VC), necrosis (N), and macrophage layer (M). Scale bar is 1 mm for A–C and 100 μm for D.

peutic effects, proliferation activities, grade of malignancy, and prognosis based on the glucose metabolism of a variety of tumors (*25–27*). As for breast cancer, Adler et al. (*28*) reported that FDG uptake correlated with the histologic grade of malignancy. In tumor cells, deoxyglucose is similarly phosphorylated by intracellular hexokinase enzyme but is not further metabolized and trapped in cells as deoxyglucose-6 phosphate. Therefore, the level of glycolysis in the tissue can be measured by the accumulation of FDG or ^{14}C-DG.

In this study, we used 3 mouse breast cancer models with different growth rates and radiosensitivities. In our tumor uptake study of FDG and ^{99m}Tc-MIBI, FDG showed a higher uptake than did ^{99m}Tc-MIBI, and the difference between the 3 tumors was significant with FDG but not with ^{99m}Tc-MIBI (Table 1). Biologic studies have shown that FDG uptake correlates with the growth rate of cancer cells (*29*) and is also a marker of viable tissues, including proliferating and nonproliferating cancer cells (*26,30*). However, ^{99m}Tc-MIBI showed a similar low uptake pattern in all tumor models. These results suggest that ^{99m}Tc-MIBI uptake is increased in neoplastic tissue but does not reflect the growth rate.

We performed ARG to investigate the intratumoral distribution pattern of ^{99m}Tc-MIBI and ^{14}C-DG in syngeneic mouse models of breast cancer. We then speculated that FM3A, MM48, and Ehrlich tumors might all be negative for P-glycoprotein expression, because accumulation of ^{99m}Tc-MIBI was observed on ARG images at 30 min after injection. We evaluated these tumors for P-glycoprotein expression by immunohistochemical staining of C219 (Signet Laboratories, Inc., Dedham, MA) according to the method of Lee et al. (*31*) and confirmed the lack of P-glycoprotein expression in all these tumors. Our results showed that the ^{99m}Tc-MIBI image had a similar distribution pattern for tumors with different growth rates (Fig. 3). However, in comparison with ^{14}C-DG, ^{99m}Tc-MIBI showed a preferential accumulation within viable cancer cells (Table 2). These results support clinical studies indicating that ^{99m}Tc-MIBI clearly delineates primary breast cancer within the breast parenchyma—a favorable characteristic for a scintimammographic agent. ^{14}C-DG images showed high uptake not only by cancer cells but also by connective tissue in the tumor, as has been reported (*17,20*).

In the postirradiation uptake studies (Fig. 4), FDG and ^{99m}Tc-MIBI showed a similar uptake pattern until day 4. However, a significant change in the uptake pattern of only ^{99m}Tc-MIBI was observed on day 7. The influence of radiotherapy on FDG uptake in tumors was reported to be

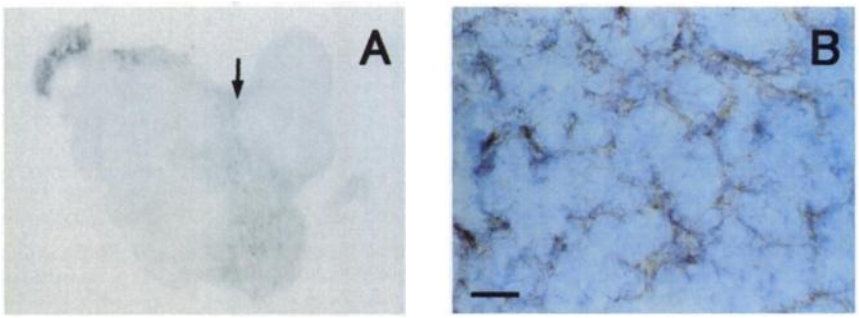

FIGURE 6. ARG image of ^{99m}Tc-MIBI (A) and immunohistochemical microvessel staining for CD34 antigen of area indicated by arrow (×400) (B). Microvessels are represented by brown cell clusters. Scale bar is 0.5 mm for A and 100 μm for B.

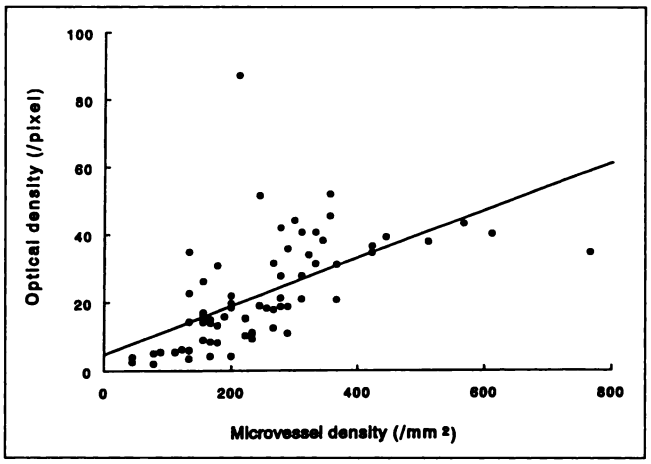

FIGURE 7. Relationship between microvessel density and optical density of ^{99m}Tc-MIBI images, by Spearman rank correlation test. Linear, significant correlation is seen.

slower than metabolic damage affecting amino acid and DNA incorporation and synthesis (*32*). Tumor growth depends on the balance between cell production and cell loss, and tumors with lower cell loss continue to grow for a couple of days after irradiation and then show a gradual shrinkage. Thus, tumor volume can be influenced by either edematous swelling or the collapse of dying tissue. Therefore, the volumetric tumor growth rate does not directly reflect the tumor growth fraction, especially after therapeutic intervention (*32*). In this study, we could not show the mechanisms of metabolic damage after irradiation, but we showed the feasibility of ^{99m}Tc-MIBI to monitor the effect of radiotherapy. These results suggest that regrowth of tumors after radiotherapy can be detected as an earlier increase in ^{99m}Tc-MIBI uptake than in FDG uptake, preceded by tumor enlargement. We evaluated the effects of a single high dose of radiation, and further study with fractionated radiation simulating the clinical setting is warranted.

We found a unique variable distribution pattern between ^{99m}Tc-MIBI and ^{14}C-DG ARG images of irradiated tumors (Fig. 5). In pretreatment studies using FM3A tumors, we previously showed that deoxyglucose accumulates not only in tumor cells but also in inflammatory cell elements in association with tumor growth or necrosis (*17*). Our results showed low ^{99m}Tc-MIBI uptake in areas damaged by irradiation, in contrast to areas with little or no damage. Radiation triggers a series of degenerative and cytolytic changes, finally leading to cell necrosis (*21*). Furthermore, ^{99m}Tc-MIBI accumulated in viable cancer cells but not in areas containing fibroblasts and infiltrating macrophages in conjunction with the elimination of dead cells from postradiotherapy necrosis. Although ^{14}C-DG uptake by viable cancer cells is significantly high, differentiation of viable cancer cells might be difficult because ^{14}C-DG uptake in the macrophage layer around necrotic areas is equal to that in viable cancer cells (*33*). Enhanced glycolysis, which is characteristic of malignancy, is a signal of macrophage activation (*34*). Tumor irradiation is usually associated with inflammatory cells; therefore, ^{14}C-DG uptake may continue and show almost homogeneous density on ARG, a pattern different from that of ^{99m}Tc-MIBI.

It has been proposed that tumor growth depends on angiogenesis and that the development of new capillaries precedes in vivo proliferation of tumor cells (*35*). In addition, several clinical studies have shown that the degree of angiogenesis, quantified by immunohistochemical staining for CD34, correlates with the incidence of distant metastases and survival rate (*13,18,19*). Figure 7 showed a significant correlation between the optical density of ^{99m}Tc-MIBI ARG and the density of microvessels in histologic sections stained for CD34. Our findings suggest that angiogenesis is important for intratumoral accumulation of ^{99m}Tc-MIBI. These results are consistent with the known characteristics of ^{99m}Tc-MIBI imaging: that ^{99m}Tc-MIBI exhibits flow-dependent distribution in the myocardium as a myocardial perfusion agent, and that tumor uptake of ^{99m}Tc-MIBI reaches a peak soon after injection, suggesting flow dependency. Accumulation of ^{99m}Tc-MIBI in tumors depends on several factors related to tumor cells, including a high number of mitochondria, a high membrane potential, and expression of the *mdr* gene (*25*). In addition to these factors, we believe that microvessel density is important in determining ^{99m}Tc-MIBI tissue accumulation.

Our results show a close relationship between the optical density of ^{99m}Tc-MIBI ARG and microvessel density. This finding suggests that a high ^{99m}Tc-MIBI uptake reflects a high density of microvessels; hence, accumulation of ^{99m}Tc-MIBI may be a useful prognostic indicator of the likelihood of metastasis and survival in breast cancer patients. This suggestion in turn implies that ^{99m}Tc-MIBI scintimammography may be useful for selecting or following up patients who receive aggressive therapy and for predicting the prognosis of breast cancer patients.

CONCLUSION

Using 3 mouse models of breast tumors having different characteristics, we showed a significantly different pattern of FDG uptake, whereas ^{99m}Tc-MIBI uptake was similar and low for all tumors and did not reflect the tumor growth rate. In ARG studies, ^{99m}Tc-MIBI showed a preferential accumulation in cancer cells but not in infiltrating fibroblasts and macrophages, and a similar intratumoral distribution pattern was seen for all 3 tumor types. Compared with ^{14}C-DG, ^{99m}Tc-MIBI preferentially and significantly accumulated in viable cancer cells for all tumor models. Postirradiation tumor uptake studies showed tumor regrowth after radiotherapy. This phenomenon was detected as an early increase in ^{99m}Tc-MIBI uptake relative to FDG uptake and was preceded by tumor enlargement. The therapeutic effect of irradiation might be evaluated by changes in ^{99m}Tc-MIBI uptake. ^{99m}Tc-MIBI uptake by tumor tissue on ARG correlated with microvessel density, indicating that tumor angiogenesis contributes to the enhanced uptake of ^{99m}Tc-MIBI. We have used animal models of tumors in our experiments.

Further studies are warranted to establish the applicability of our findings to human tumors. We hope our results will be clinically useful and further enhance ^{99m}Tc-MIBI scintimammography.

ACKNOWLEDGMENTS

The authors thank the staff of the Cyclotron and Radioisotope Center, Tohoku University; the Department of Pathology, Tohoku University Hospital; and the Division of Tumor Animals, Institute for Experimental Animals, for their cooperation. The authors also thank Yasuhiro Sugawara for preparation of histologic samples and Dr. Yoshikazu Sugimoto for the kind gift of the C219 monoclonal antibody. This study was supported by grants-in-aid (12470183 and 11671145) from the Ministry of Education, Science, Sports and Culture, Japan, and by Daiichi Radioisotope Laboratories, Ltd., Tokyo, Japan.

REFERENCES

1. Sondik EJ. Breast cancer trends: incidence, mortality and survival. *Cancer.* 1994;74:995–999.
2. Waxman A, Ashock G, Kooba A, et al. The use of ^{99m}Tc-methoxy isobutylisonitrile (MIBI) in the evaluation of patients with primary carcinoma of the breast. [abstract]. *Clin Nucl Med.* 1992;9:761.
3. Prats E, Aisa F, Abos MD, et al. Mammography and ^{99m}Tc-MIBI scintimammography in suspected breast cancer. *J Nucl Med.* 1999;40:296–301.
4. Joaquim AI, Sagarra AJ, Ramos CD, Coudry R, Sagarra RAM, Camargo EE. Tc-99m sestamibi scintimammography in the evaluation of response of breast carcinoma to chemotherapy. *Clin Nucl Med.* 1997;22:638–640.
5. Rao VV, Chiu ML, Kronauge JF, Piwnica-Worms D. Expression of recombinant human multidrug resistance p-glycoprotein in insect cells confers decreased accumulation of technetium-99m-sestamibi. *J Nucl Med.* 1994;35:510–515.
6. Palmedo H, Schomburg A, Grunwald F, Mallmann P, Krebs D, Biersack H. Technetium-99m-MIBI scintimammography for suspicious breast lesions. *J Nucl Med.* 1996;37:626–630.
7. Piwnica-Worms D, Chui ML, Budding M, Kronauge JF, Kramer RA, Croop JM. Functional imaging of multidrug-resistant p-glycoprotein with an organotechnetium complex. *Cancer Res.* 1993;53:977–984.
8. Kostakoglu L, Elahi N, Kiratli P, et al. Clinical validation of the influence of p-glycoprotein on technetium-99m-sestamibi uptake in malignant tumors. *J Nucl Med.* 1997;38:1003–1008.
9. Kostakoglu L, Ruacan S, Ergun EL, Sayek I, Elahi N, Bekdik CF. Influence of the heterogeneity of p-glycoprotein expression on technetium-99m-MIBI uptake in breast cancer. *J Nucl Med.* 1998;39:1021–1026.
10. Bosari S, Lee AK, DeLellis RA, et al. Microvessel quantification and prognosis in invasive breast carcinoma. *Hum Pathol.* 1992;23:755–761.
11. Weidner N, Semple JP, Welch WR, Folkman J. Tumor angiogenesis and metastasis: correlation in invasive breast carcinoma. *N Engl J Med.* 1991;324:1–8.
12. Weidner N, Folkman J, Pozza F, et al. Tumor angiogenesis: a new significant and independent prognostic indicator in early-stage breast carcinoma. *J Natl Cancer Inst.* 1992;84:1875–1887.
13. Simpson JF, Ann C, Battifora H, Esteban JM. Endothelial area as a prognostic indicator for invasive breast carcinoma. *Cancer.* 1996;77:2077–2085.
14. Kubota K, Matsuzawa T, Takahashi T, et al. Rapid and sensitive response of carbon-11-L-methionime tumor uptake to irradiation. *J Nucl Med.* 1989;30:2012–2016.
15. Ishiwata K, Ido T, Nakanishi H, Iwata R. Contamination of 2-deoxy-2-[^{18}F]fluoro-D-mannose in the 2-deoxy-2-[^{18}F]fluoro-D-glucose preparations synthesized from [^{18}F]acetyl hypofluoride and [^{18}F]F_2. *Appl Radiat Isot.* 1987;38:463–466.
16. Kubota R, Kubota K, Yamada S, et al. Methionine uptake by tumor tissue: a microautoradiographic comparison with FDG. *J Nucl Med.* 1995;36:484–492.
17. Kubota R, Yamada S, Kubota K, Ishiwata K, Tamahashi N, Ido T. Intratumoral distribution of fluorine-18-fluorodeoxyglucose in vivo: high accumulation in macrophages and granulation tissues studied by microautoradiography. *J Nucl Med.* 1992;33:1972–1980.
18. Tomisaki S, Ohno S, Ichiyoshi Y, Kuwano H, Maehara Y, Sugimachi K. Microvessel quantification and its possible relation with liver metastasis in colorectal cancer. *Cancer.* 1996;77:1722–1726.
19. Obermair A, Tempfer C, Wasicky R, Kaider A, Hefler L, Kainz C. Prognostic significance of tumor angiogenesis in endometrial cancer. *Obstet Gynecol.* 1999;93:367–371.
20. Yamada S, Kubota K, Kubota R, et al. High accumulation of fluorine-18-fluorodeoxyglucose in turpentine-induced inflammatory tissue. *J Nucl Med.* 1995;36:1301–1306.
21. Shimosato Y, Oboshi S, Baba K. Histological evaluation of effects of radiotherapy and chemotherapy for carcinoma. *Jpn J Clin Oncol.* 1971;1:19–35.
22. Chiu ML, Kronauge JF, Piwnica-Worms D. Effect of mitochondrial and plasma membrane potentials on accumulation of hexakis (2-methoxyisobutylisonitrile) technetium(I) in cultured mouse fibroblasts. *J Nucl Med.* 1990;31:1646–1653.
23. Moretti JL, Caglar M, Boaziz C, Calliat-Vigneron N, Morere JF. Sequential functional imaging with technetium-99m hexakis-2-methoxyisobutylisonitrile and indium-111 octreotide: can we predict the response to chemotherapy in small cell lung cancer? *Eur J Nucl Med.* 1995;22:177–180.
24. Maffioli L, Steens J, Pauwels E, Bombardieri E. Applications of ^{99m}Tc-sestamibi in oncology. *Tumori.* 1996;82:12–21.
25. Palmedo H, Bender H, Grunwald F, et al. Comparison of fluorine-18 fluorodeoxyglucose positron emission tomography and technetium-99m methoxyisobutylisonitrile scintimammography in the detection of breast tumors. *Eur J Nucl Med.* 1997; 24:1138–1145.
26. Oshida M, Uno K, Suzuki M, et al. Predicting the prognoses of breast carcinoma patients with positron emission tomography using 2-deoxy-2-fluoro[^{18}F]-D-glucose. *Cancer.* 1998;82:2227–2234.
27. Bassa P, Kim E, Inoue T, et al. Evaluation of preoperative chemotherapy using PET with fluorine-18-fluorodeoxyglucose in breast cancer. *J Nucl Med.* 1996;37: 931–938.
28. Adler LP, Crowe JP, Al-Kaishi NK, Sunshine JL. Evaluation of breast masses and axillary lymph nodes with [F-18]2-deoxy-2 fluoro-D-glucose PET. *Radiology.* 1993;187:743–750.
29. Minn H, Clavo AC, Grenman R, Wahl RL. In vitro comparison of cell proliferation kinetics and uptake of tritiated fluorodeoxyglucose and L-methionine in squamous cell carcinoma of the head and neck. *J Nucl Med.* 1995;36:252–258.
30. Kubota K, Kubota R, Yamada S. FDG accumulation in tumor tissue. *J Nucl Med.* 1993;34:419–421.
31. Lee GY, Croop JM, Anderson E. Multidrug resistance gene expression correlates with progesterone production in dehydroepiandrosterone-induced polycystic and equine chorionic gonadotropin-stimulated ovaries of prepubertal rats. *Biol Reprod.* 1998;58:330–337.
32. Kubota K, Iwashita K, Kubota R, et al. Tracer feasibility for monitoring of tumor radiotherapy: a quadruple tracer study with ^{18}F-FDG or ^{18}F-FdUrd, ^{14}C-Met, ^{3}H-Thd and ^{67}Ga. *J Nucl Med.* 1991;32:2118–2123.
33. Reinhardt MJ, Kubota K, Yamada S, Iwata R, Yaegashi H. Assessment of cancer recurrence in residual tumors after fractionated radiotherapy: a comparison of fluorodeoxyglucose, L-methionine and thymidine. *J Nucl Med.* 1997;38:280–287.
34. Bustos R, Sobrino F. Stimulation of glucolysis as an activation signal in rat peritoneal macrophages. *Biochem J.* 1992;282:299–303.
35. Folkman J. What is the evidence that tumors are angiogenesis dependent? *J Natl Cancer Inst.* 1990;82:4–6.